JOURNAL OF THERMOPHYSICS AND HEAT TRANSFER
Vol. 6, No. 4, Oct.–Dec. 1992

Bidirectional Reflectance and Specularity of Twelve Spacecraft Thermal Control Materials

B. L. Drolen*
Hughes Aircraft Company, Los Angeles, California 90009

Many spacecraft external payloads are sensitive to focused solar heating caused by specular reflections from exterior thermal control surfaces. This paper presents a method of calculating specularity using bidirectional reflectance distribution function (BRDF) input. Definitions are presented for directional and hemispherical specularity as a function of the conical half-angle surrounding the specular ray. Measured BRDF data are presented for commonly used thermal control materials including plastic films and paints. Angles of incidence range from 5 to 78 deg and data are taken both in and out of the plane of incidence. Most measurements are made at a wavelength of 0.488 μm, though measurements for two white paints are also made at 1.06, 3.39, and 10.63 μm. The BRDF values are found to increase with both angle of incidence and wavelength. A numerical code is described that integrates BRDF data to yield both directional and hemispherical specularity as a function of cone half-angle around the specular ray. Specularity results are presented for all 12 materials studied.

Nomenclature

β = zenith angle in specular ray coordinates, deg
θ = zenith angle in normal spherical coordinates, deg
λ = wavelength, μm
ν = azimuthal angle in specular ray coordinates, deg
ρ = reflectance
$\overline{\rho_b}$ = constant base reflectance within specular cone
σ = specularity
ϕ = azimuthal angle in normal spherical coordinates, deg
ω, Ω = solid angles

Subscripts
b = diffuse
c = critical
dh = directional-hemispherical
h = hemispherical
hd = hemispherical-directional
i = incident
m = specular
o = normal
r = reflected
λ = spectral

Superscripts
$''$ = bidirectional
$'$ = directional

Introduction

SPACECRAFT thermal engineers require various radiative surface properties to calculate environmental heating rates and radiative interchange factors. These properties include infrared emittance, solar absorptance, and specularity (where specularity is a measure of the non-diffuse characteristics of the reflecting surface). Some spacecraft thermal control surfaces, such as flat paints and quartz mirrors, may be approximated as being fully diffuse or fully specular. However, many materials (e.g., glossy paints and embossed silver Teflon®) exhibit partially diffuse or partially specular reflectance characteristics. In this case, the diffuse-plus-specular model of surface reflectance postulated by Seban[1] is typically employed. Despite wide acceptance of this model, little progress has been made regarding the appropriate value of σ, for common spacecraft thermal control surfaces. The thermal engineer resorts to bounding and parametric cases to determine if reflected incidence is a problem.

Bobco and Drolen[2] presented a technique for calculating surface specularity and applied it to a bimodal model of bidirectional reflectance. The work reported here extends that technique for application to measured BRDF data. There is little published BRDF data for spacecraft thermal control materials. Most published BRDF data are for specially prepared surfaces with controlled surface characteristics.[3–7] These data are useful for correlating analytical BRDF models but are of little quantitative value in spacecraft applications. Reported experimental measurements of bidirectional reflectance often mask the absolute values of BRDF. Data are normalized or scaled by the value at the peak, the value along the specular direction, or the value normal to the surface; in many cases the absolute value at the peak is not reported, making the transformation back to BRDF impossible. Funai[8] presents results for a variety of thermal control materials in the form of a relative detected signal strength. Conversion to a measured BRDF value does not appear possible, making the data only qualitatively useful. Miller[9] reported BRDF values for six thermal control materials, including one precursor to a material tested here, S-13 white paint.

This article presents the analytical tools to integrate BRDF data to determine specularity. It describes the experimental facility used to gather required BRDF data. Measured BRDF data are presented for commonly used thermal control materials, including plastic films and paints. A numerical code is described that integrates BRDF data to yield directional and hemispherical specularity as a function of cone half-angle around the specular ray. Specularity results are presented for all twelve materials in the study as a function of cone half-angle from the specular ray.

Background

The reflective characteristics of a surface are described by its bidirectional reflectivity ρ''_λ. The bidirectional reflectivity[10] is a ratio of the reflected intensity in direction (θ_r, ϕ_r) to the energy incident from direction (θ_i, ϕ_i):

$$\rho''_\lambda(\theta_r, \phi_r, \theta_i, \phi_i) = \frac{i''_{\lambda r}(\theta_r, \phi_r, \theta_i, \phi_i)}{i'_{\lambda i}(\theta_i, \phi_i)\cos\theta_i \, d\omega_i}, \ (\mathrm{sr}^{-1}) \qquad (1)$$

Received April 12, 1991; presented as Paper 91-1326 at the AIAA 26th Thermophysics Conference, Honolulu, HI, June 24–26, 1991; revision received Oct. 28, 1991; accepted for publication Oct. 29, 1991.

*Senior Staff Engineer, Space and Communications Group. Member AIAA.

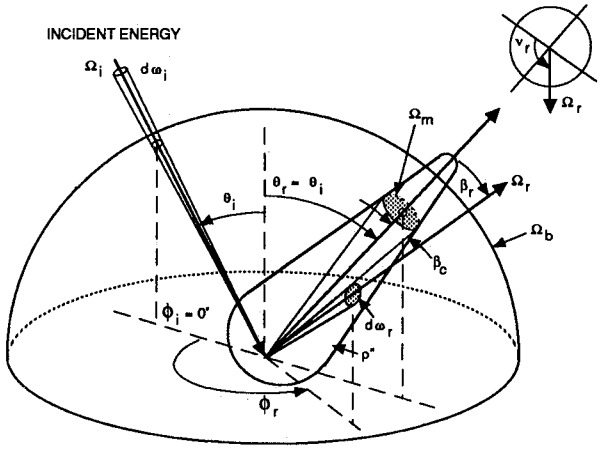

Fig. 1 Coordinate system for bidirectional reflectance and specularity.

It is a function of the incident and reflected angles, the solid angle of the incident energy, and the incident wavelength. It also depends on surface temperature and polarization, but these effects are not considered in the present analysis. For the remainder of the analysis section the λ subscript is omitted. The bidirectional reflectivity is also referred to as the bidirectional reflectance distribution function, or BRDF. Figure 1 depicts the geometry of the incoming and reflecting energy, showing angles θ_i, ϕ_i, θ_r, and ϕ_r as well as the respective solid angles.

The directional-hemispherical reflectance ρ'_{dh}, hemispherical-directional reflectance ρ'_{hd}, and hemispherical reflectance ρ_h, are each derivable given ρ''[10]:

$$\rho'_{dh}(\theta_i, \phi_i) = \int_{(2\pi)_r} \rho''(\theta_r, \phi_r, \theta_i, \phi_i)\cos\theta_r \, d\omega_r \tag{2}$$

$$\rho'_{hd}(\theta_r, \phi_r) = \int_{(2\pi)_i} \rho''(\theta_r, \phi_r, \theta_i, \phi_i)\cos\theta_i \, d\omega_i \tag{3}$$

$$\rho_h = \frac{1}{\pi}\int_{(2\pi)_i} \rho'_{dh}(\theta_i, \phi_i)\cos\theta_i \, d\omega_i \tag{4a}$$

$$\rho_h = \frac{1}{\pi}\int_{(2\pi)_r} \rho'_{hd}(\theta_r, \phi_r)\cos\theta_r \, d\omega_r \tag{4b}$$

Seban[1] decomposed hemispherical reflectance into specular and diffuse components

$$\rho_h = \rho_m + \rho_d \tag{5}$$

The NEVADA Monte-Carlo ray trace program, in common use by spacecraft thermal control engineers, incorporates σ, that is the fraction of reflected energy in the specular direction

$$\sigma = \rho_m/\rho_h \tag{6}$$

The primary goal of this article is to provide meaningful values for this parameter's use in spacecraft thermal control analyses. In the following analysis, the definition is broadened somewhat to include energy in the near-specular direction. In the analysis of optical systems it may be important to quantify the portion of the energy that is precisely along the specular ray ($\Delta\omega_r = 0$). However, for thermal analysis it is less important to know whether an image can be resolved and more important to ensure that all of the energy reflected from a surface is accurately accounted for and equitably distributed.

Analysis

Bidirectional reflectance data often show a peak value at or near the specular direction with a lower, more uniform value outside a finite solid angle surrounding the peak. This observation suggests that the half-space for reflected energy can be decomposed into 2 solid angles $\Omega_m + \Omega_b = (2\pi)_r$, where solid angle Ω_m includes the specular direction and Ω_b is the remainder of the half-space (Fig. 1). Define ρ''_m and ρ''_b equal to ρ'' in the respective solid angles and assume the existence of $\overline{\rho_b}$ in Ω_m, where $\overline{\rho_b}$ is a constant equal to the minimum value of ρ'' at the intersection of Ω_m and Ω_b. Then, the directional-hemispherical and hemispherical reflectances become

$$\rho'_{dh}(\theta_i, \phi_i) = \int_{\Omega_m} (\rho''_m - \overline{\rho_b})\cos\theta_r \, d\omega_r + \int_{(2\pi)_r} \rho''_b \cos\theta_r \, d\omega_r \tag{7}$$

$$\pi\rho_h = \int_{(2\pi)_i}\left[\int_{\Omega_m} (\rho''_m - \overline{\rho_b})\cos\theta_r \, d\omega_r\right]\cos\theta_i \, d\omega_i + \int_{(2\pi)_i}\left(\int_{(2\pi)_r} \rho_b \cos\theta_r \, d\omega_r\right)\cos\theta_i \, d\omega_i \tag{8}$$

The specular components of the directional hemispherical reflectance ρ'_m, and the hemispherical reflectance ρ_m, can then be defined as follows:

$$\rho'_m = \int_{\Omega_m} (\rho''_m - \overline{\rho_b})\cos\theta_r \, d\omega_r \tag{9}$$

$$\rho_m = \frac{1}{\pi}\int_{(2\pi)_i}\left[\int_{\Omega_m} (\rho''_m - \overline{\rho_b})\cos\theta_r \, d\omega_r\right]\cos\theta_i \, d\omega_i \tag{10}$$

Note that Seban's decomposition of hemispherical reflectance[1] is extended here to directional hemispherical reflectance as well. In many design cases, the angle of incidence upon an illuminated surface is a known, fixed value, and the first reflection off of this surface accounts for most of the energy reflecting from it to the other surfaces in the system. In these cases it would be inappropriate to use a specularity that had been integrated over θ_i from 0 to 90 deg. Instead, BRDF data for the actual angle of incidence need only be integrated over the reflection angles. The specular component is then that part of the directional-hemispherical reflectance in Ω_m. A directional specularity can then be defined as

$$\sigma' = \rho'_m/\rho'_{dh} \tag{11}$$

Note that the hemispherical specular component is related to the directional specular component by

$$\rho_m = \frac{1}{\pi}\int_{(2\pi)_i} \rho'_m \cos\theta_i \, d\omega_i \tag{12}$$

Equations (9) and (10) can be used to calculate the specular components when given BRDF data and an appropriate choice for Ω_m. The choice of Ω_m requires engineering judgment and is dependent upon the geometric configuration of the system being analyzed. A good choice of relevant Ω_m for reflection from a given surface to another would be related to the view factors between the two surfaces.

Equations (7–10) highlight the need for integration over a conical solid angle located around the specular ray. In standard spherical coordinates (axis normal to the surface), this integration is cumbersome for all cases except normal incidence. The natural coordinates for this integration are a "tilted spherical" system with the axis along the specular ray (Fig. 1). In this system β_r is the off-specular angle, ν_r is the azimuthal angle about the specular ray, and the differential solid angle becomes

$$d\omega_r = \sin\beta_r \, d\beta_r \, d\nu_r \tag{13}$$

A standard transformation of variables leads to an expression for the cosine of θ_r in the new coordinates

$$\cos\theta_r = \sin\theta_i \sin\beta_r \cos\nu_r + \cos\beta_r \cos\theta_i \quad (14)$$

Transformation of Eq. (9) in terms of β_r and ν_r then yields

$$\rho'_m = \int_0^{2\pi}\int_0^{\beta_c} (\rho''_m - \overline{\rho_b})(\sin\theta_i \sin\beta_r \cos\nu_r + \cos\beta_r \cos\theta_i)\sin\beta_r \, d\beta_r \, d\nu_r \quad (15)$$

If ρ''_m is independent of ν_r, Eq. (15) reduces to

$$\rho'_m = 2\pi \int_0^{\beta_c} (\rho''_m - \overline{\rho_b})\cos\beta_r \sin\beta_r \cos\theta_i \, d\beta_r \quad (16)$$

Equation (16) is useful for integrating analytical models of BRDF, most of which are independent of the azimuthal angle around the specular ray.

The new variable arising in Eqs. (15) and (16) is β_c, the conical half-angle that defines the specular solid angle Ω_m used in Eqs. (7–10). Note that if β_c is held constant for all incidence angles, the hemispherical property integrations [Eqs. (8), (10), and (12)] become undefined when $\beta_c > \pi/2 - \theta_i$ (i.e., the conical domain of integration for the specular component protrudes below the surface). To avoid this problem β_c is assumed to decrease linearly from $\beta_{c,0}$ at normal incidence to zero at $\theta_i = \pi/2$, so that

$$\beta_c(\theta_i) = \beta_{c,o}(1 - 2\theta_i/\pi) \quad (17)$$

in the integration over incidence angle for hemispherical specularity. An alternative to this assumption is to keep β_c fixed for all angles of incidence but to truncate the hemispherical integrations at $\beta_c = \pi/2 - \theta_i$. Doing so leads to the unacceptable omission of a significant portion of the hemispherical integrals, especially for large cone half-angles.

Some real surfaces display off-specular peaks in their BRDF. The above analysis does not account for this effect. The integration proceeds in spherical caps surrounding the ideal specular ray. Inasmuch as the output specularity is to be used in diffuse-plus-specular modeling, this is a consistent limitation to the analysis.

BRDF Facility and Sample Description

The samples chosen for this investigation are commonly used spacecraft thermal control materials. Table 1 describes the test samples and the wavelengths at which the measurements were made. The sample set includes materials that span the range of specularity from nearly diffuse flat paints, through textured materials with moderate specularity, to highly specular second-surface metallized plastic films. The samples were produced under flight-typical material and process specifications to obtain samples as flight-like as possible. Of the twelve samples, three are described further here, since they are not in wide use. The black Kapton material, used for the outer layers of multilayer insulation (MLI) blankets, is carbon-filled to preclude space-charging problems. The reinforced black Kapton material incorporates a 0.635 × 0.635 cm mesh of Nomex on the backside for added strength to avoid tearing. The mesh pattern is exhibited on the front side as a macroscopic grid. The embossed, silvered Teflon material is typical of the film used on the space transportation system (STS) thermal radiators. The samples were applied to 7.62 × 7.62 × 0.254 cm aluminum plates the surface roughness and flatness of which were not precisely controlled. Qualitatively, each mounting plate was flat when resting on a flat plate, and the roughness was that of typical aluminum sheet.

Figure 2 is a schematic of the facility used for the BRDF measurements.[11] The four lasers used for these measurements are as follows: argon ion (0.4545–0.5145 μm circularly polarized); neodymium: YAG (1.06 μm randomly polarized); IR helium-neon (3.39 μm vertically polarized); and carbon dioxide (9.2–11.0 μm circularly polarized). Most of the data presented here were taken at a wavelength of 0.488 μm using the argon ion laser and should be representative of specularity in the visible portion of the spectrum. The S13-GLO and zinc orthotitanate (ZOT) white paint samples, reasonably diffuse in the visible, were measured at four wavelengths: 0.488 μm, 1.06 μm (S13-GLO only), 3.39 μm, and 10.63 μm, which shows the effect of increasing wavelength on the specularity of visibly diffuse white paints. The beam diameter was small (~5 mm) to keep the illuminated spot size small (<2.54 cm) at near-grazing incidence. A chopper and reference detector are included in the beam path to continuously monitor and correct for drift in source output power. The solid angles of incidence and reflection are identical 5×10^{-5} sr. BRDF values were calculated using Eq. (1). Previous measurements with this facility indicate an approximate accuracy of about ±10% in the visible and ±20% in the infrared.

The samples were mounted on a computer-controlled four-axis radiometric goniometer. This goniometer is an assembly of four stepper-motor-driven, computer programmable turntables and two manually operated translation stages. Angular accuracy for all DOG is 0.1 deg or better, with 0.01 deg repeatability. A coordinate transformation is performed to translate the laboratory coordinates controlled by the goniometer into the sample coordinates that have physical significance for the BRDF. A set of 291 incident-reflected angle pairs was measured for each sample, representing a thorough in- and out-of-plane investigation of the BRDF. This set included five angles of incidence from near-normal (5 deg) to near-grazing (78 deg) in uniform steps of cosine to aid integration. The azimuthal incidence angle ϕ_i was maintained at 0 deg for all measurements. The zenith reflected angle θ_r was varied in eight uniform steps in cosine, and the azimuthal reflected angle ϕ_r was varied over eight positions from 0–180 deg, concentrating more closely on the forward reflected direction (near 180 deg). Measurements were also taken at the specular peak, that, for each of the materials showing any specular behavior, occurred at or very close to the specular angle. Additional BRDF measurements were taken for the more specular samples at incident-reflected angle pairs near the specular peak. These included measurements at 1, 3, 5, and 7 deg from the ideal specular direction.

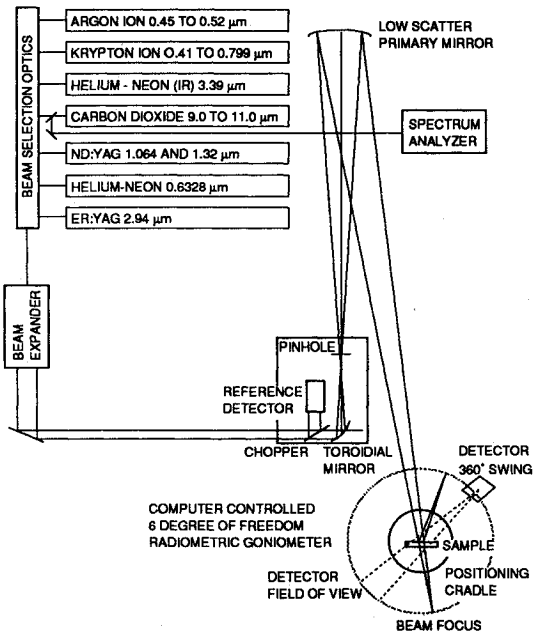

Fig. 2 BDRF measurement facility configuration.

Table 1 Specularity results

Sample description	Measurement wavelength, μm	$\beta_{c,o}$, deg	Directional specularity θ_i = 5 deg	θ_i = 37 deg	θ_i = 53 deg	θ_i = 66 deg	θ_i = 78 deg	σ hemi	ρ hemi
Black Kapton, 25.4 μm	0.488	4	0.052	0.056	0.103	0.165	0.334	0.151	
		10	0.248	0.196	0.284	0.396	0.725	0.410	0.18
		20	0.571	0.396	0.457	0.587	0.852	0.620	
Reinforced black Kapton, 25.4 μm	0.488	4	0.063	0.037	0.067	0.082	0.024	0.052	
		10	0.284	0.133	0.234	0.240	0.142	0.193	0.15
		20	0.523	0.328	0.465	0.434	0.419	0.422	
ITO/Kapton/Al, 25.4 μm	0.488	4	0.633	0.699	0.620	0.621	0.441	0.628	
		10	0.817	0.903	0.882	0.844	0.785	0.853	0.11
		20	0.964	0.949	0.942	0.929	0.891	0.938	
Kapton/Al, 12.7 μm	0.488	4	0.302	0.446	0.314	0.244	0.160	0.298	
		10	0.428	0.799	0.787	0.648	0.605	0.606	0.27
		20	0.538	0.912	0.944	0.885	0.848	0.798	
Teflon/Ag, 127 μm	0.488	4	0.627	0.702	0.675	0.510	0.367	0.596	
		10	0.698	0.771	0.776	0.731	0.808	0.757	0.49
		20	0.838	0.806	0.820	0.784	0.908	0.833	
Embossed Teflon/Ag, 127 μm	0.488	4	0.018	0.006	0.005	0.002	0.001	0.007	
		10	0.196	0.062	0.032	0.025	0.012	0.074	0.76
		20	0.780	0.375	0.208	0.147	0.063	0.390	
Black gloss Chemglaze paint, Z302	0.488	4	0.814	0.782	0.846	0.844	0.778	0.807	
		10	0.833	0.817	0.888	0.922	0.969	0.920	0.06
		20	0.869	0.825	0.895	0.933	0.987	0.939	
Black flat Chemglaze paint, Z306	0.488	4	0.000	0.000	0.000	0.000	0.000	0.000	
		10	0.001	0.002	0.002	0.001	0.000	0.001	0.09
		20	0.013	0.014	0.011	0.005	0.002	0.010	
White gloss Chemglaze paint, A276	0.488	4	0.033	0.035	0.046	0.060	0.052	0.042	
		10	0.055	0.051	0.072	0.102	0.130	0.069	0.82
		20	0.136	0.062	0.084	0.117	0.179	0.100	
White flat Chemglaze paint	0.488	4	0.000	0.000	0.000	0.000	0.000	0.000	
		10	0.000	0.000	0.000	0.000	0.001	0.000	0.83
		20	0.004	0.002	0.003	0.003	0.004	0.003	
Zinc orthotitanate white paint	0.488	4	0.000	0.000	0.000	0.000	0.000	0.000	
		10	0.001	0.000	0.000	0.000	0.000	0.000	0.85
		20	0.009	0.001	0.000	0.000	0.000	0.002	
	3.39	4	0.000	0.000	0.001	0.012	0.053	0.010	
		10	0.005	0.001	0.005	0.042	0.205	0.037	0.18
		20	0.010	0.005	0.018	0.091	0.331	0.071	
	10.63	4	0.070	0.134	0.291	0.492	0.101	0.262	
		10	0.162	0.261	0.491	0.642	0.394	0.443	0.03
		20	0.347	0.332	0.571	0.721	0.580	0.553	
S13-GLO white paint	0.488	4	0.000	0.000	0.000	0.000	0.000	0.000	
		10	0.001	0.000	0.000	0.000	0.000	0.000	0.87
		20	0.005	0.001	0.001	0.000	0.002	0.002	
	1.06	4	0.000	0.000	0.000	0.000	0.000	0.000	
		10	0.001	0.000	0.000	0.000	0.001	0.000	0.85
		20	0.009	0.000	0.000	0.001	0.005	0.003	
	3.39	4	0.001	0.001	0.001	0.003	0.006	0.003	
		10	0.005	0.008	0.014	0.032	0.054	0.024	0.09
		20	0.031	0.039	0.069	0.136	0.191	0.100	
	10.63	4	0.025	0.014	0.041	0.119	0.242	0.096	
		10	0.202	0.128	0.173	0.327	0.607	0.325	0.06
		20	0.655	0.400	0.424	0.568	0.768	0.596	

BRDF Results

Figure 3 presents BRDF results for the following samples: black Kapton (25.4-μm thick), indium-tin-oxide (ITO)/Kapton/Al (25.4-μm thick), Teflon/Ag (127-μm thick), embossed Teflon/Ag (127-μm thick), Chemglaze white paint (flat and gloss), and S13-GLO white paint (measured at wavelengths of 0.488 and 10.63 μm). For ease of visualization, the results shown here are the in-plane data only. In general, the out-of-plane data, $0 < \phi_i < 180$ deg, exhibited quasi-isotropic behavior, i.e., smooth transition between the in-plane data at equal β angles from the specular peak. The abscissa for each figure is shown as the angle from the ideal specular ray in the incidence plane. Negative angles indicate that the reflection is back toward the source from the specular ray.

The profile of the data for black Kapton (Fig. 3a) is representative of that for each of the plastic films. The value at the specular peak grows with incidence angle, the specular peak occurs at the ideal specular angle, and there is no obvious transition from a sharp specular profile to a flat diffuse profile. Because of first-surface reflection, black Kapton, even with its strong absorption at this wavelength, exhibits a high specular peak. The reinforced black Kapton BRDF profiles are similar to those of the unreinforced, with the exception of a more jagged profile at increased incidence angle. The results for ITO-coated aluminized Kapton (Fig. 3b) are similar to those of the black Kapton. The peak is somewhat more pronounced, with most data above a value of 1 sr^{-1} occurring within 10 deg of the specular angle, compared to 15 deg for black Kapton. The results for silvered Teflon (Fig. 3c) indicate an even narrower specular peak and a flat profile with relatively high reflectance in the off-specular directions ($\beta > 60$ deg). This behavior is most likely due to Rayleigh scattering in the Teflon layer that gives it a characteristic bluish cast when viewed in room light. The measurements made at 0.488 μm would be sensitive to this effect. Figure 3d shows the BRDF profiles for the embossed silvered Teflon sample. The peaks are much broader, and the peak values are reduced approximately 100-fold from those for the unembossed sample. The relatively constant values measured in the neigh-

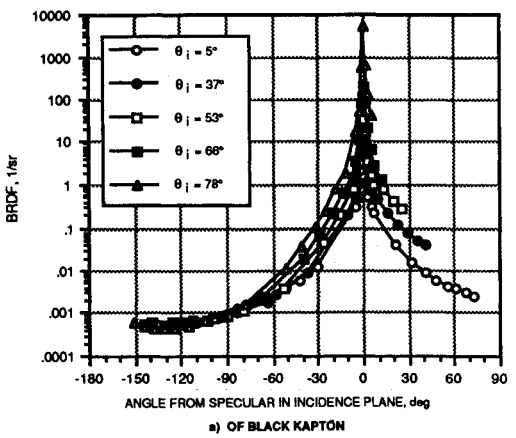

a) OF BLACK KAPTON

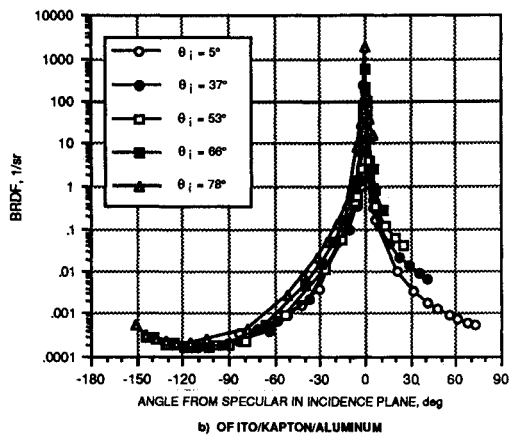

b) OF ITO/KAPTON/ALUMINUM

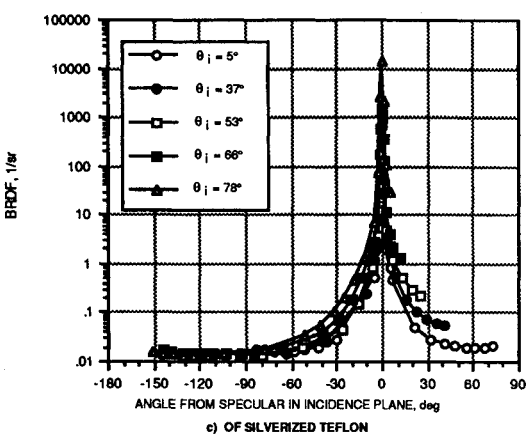

c) OF SILVERIZED TEFLON

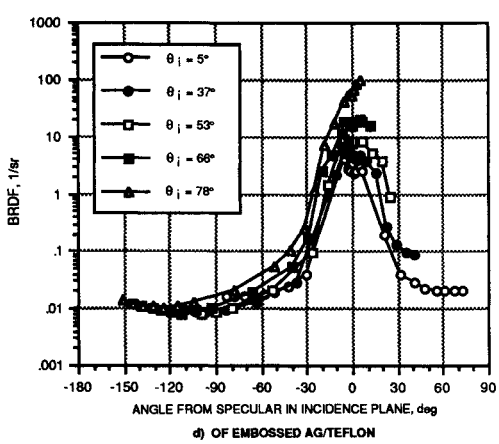

d) OF EMBOSSED AG/TEFLON

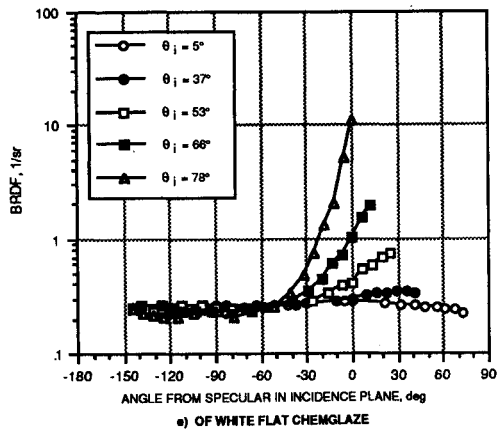

e) OF WHITE FLAT CHEMGLAZE

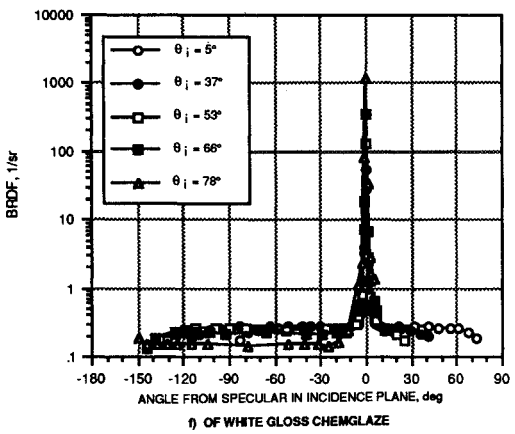

f) OF WHITE GLOSS CHEMGLAZE

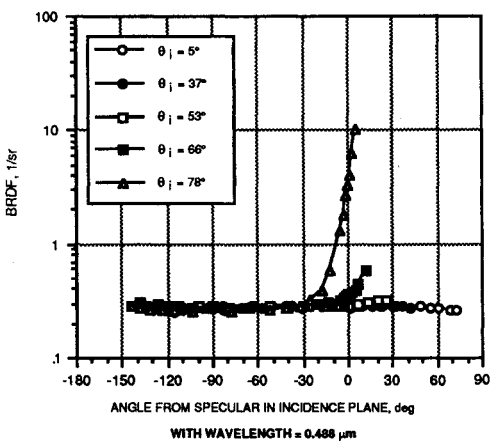

g) OF S13-GLO PAINTED ALUMINUM

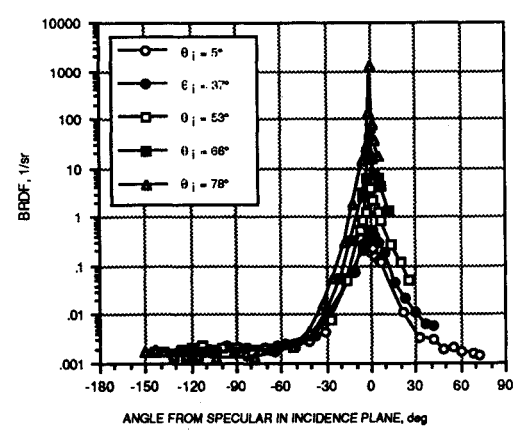

h) OF S13-GLO PAINTED ALUMINUM

Fig. 3 Measured bidirectional reflectance.

borhood of the peak would be well represented by the bimodal model.[2]

The white flat Chemglaze paint (Fig. 3e) shows diffuse behavior at near-normal incidence, but the value at the peak increases by a factor of 30 at near-grazing incidence. Notice that the peak does not occur at the specular angle and, in fact, due to instrument limitations, the peak is not resolved for angles of incidence greater than 37 deg. This off-specular behavior is reminiscent of that shown by Torrance and Sparrow[5] for a MgO sample at similar wavelengths. Figure 3f shows BRDF profiles for white gloss Chemglaze. The narrow peak and flat off-specular behavior make this material a good candidate for the diffuse-plus-specular model. The same conclusion holds for the black gloss Chemglaze paint. The white gloss sample displayed no off-specular behavior; in fact, the flat portion of the profile appears to be nearly constant on either side of the specular peak. The BRDF value of the flat portion of the white gloss Chemglaze is high (0.15–0.3 sr^{-1}). Even without a peak to consider in the integration for directional-hemispherical reflectance, this level of BRDF would yield a ρ'_{dh}, or πX BRDF, between 0.47 and 0.94, indicating that most of the integrated reflectance is in the diffuse portion rather than specular. In contrast, the black gloss paint has a low BRDF away from the specular peak. This indicates that the flat behavior is due to subsurface scattering, which is pronounced for white pigment and small for black pigment.

Figures 3g and 3h show the BRDF for S13-GLO white paint at $\lambda = 0.488$ μm and $\lambda = 10.63$ μm, respectively. The 0.488 μm data are similar to those obtained for white flat Chemglaze (Fig. 3e) except that the BRDF for S13-GLO remains flat to higher angles of incidence (53 deg as compared to 37 deg). At 10.63 μm the BRDF appears as specular as that of black Kapton (see Fig. 3a). The BRDF shape at 1.06 μm is virtually unchanged from that at 0.488 μm, while at 3.39 μm, the transition to specular has begun. These results indicate the need for care in extending experience in the visible to analyses in the IR.

Numerical Integration of BRDF Data

BRDF data can be numerically integrated to yield ρ'_{dh}, ρ_h, ρ'_m, and ρ_m by means of key approximations. Introducing $\mu_r = \cos\theta_r$ and $\mu_i = \cos\theta_i$ and assuming 1) symmetry in ϕ_r about the plane of incidence, and 2) isotropy in ϕ_i enables Eqs. (7), (8), (12), and (16) to be reduced to the following:

$$\rho'_{dh} = 2\int_0^{\pi}\int_0^{1} \rho'' \mu_r \, d\mu_r \, d\phi_r \tag{18}$$

$$\rho_h = 2\int_0^{1} \rho'_{dh} \mu_i \, d\mu_i \tag{19}$$

$$\rho'_m = 2\int_0^{\pi}\int_0^{\beta_c} \rho''(\sin\theta_i \sin\beta_r \cos\nu_r + \cos\beta_r \cos\theta_i)\sin\beta_r \, d\beta_r \, d\nu_r \tag{20}$$

$$\rho_m = 2\int_0^{1} \rho'_m \mu_i d\mu_i \tag{21}$$

A computer code was developed to perform the above integrations, with the integrals in Eqs. (18) and (20) approximated by Simpson's rule, i.e.

$$I = \frac{\Delta X}{3}\left(f_0 + f_n + 4\sum_{\substack{j=1 \\ j \text{ odd}}}^{n-1} f_j + 2\sum_{\substack{j=2 \\ j \text{ even}}}^{n-2} f_j\right) + (\text{higher order terms}) \tag{22}$$

while those in Eqs. (19) and (21) are approximated by a simple trapezoidal quadrature. BRDF data are not often available in the uniformly spaced intervals needed by Simpson's rule. The DSURF interpolation routine of the IMSL math library[12] is used here to take the irregularly spaced BRDF input and produce a surface of regularly spaced function values. The grid spacing is an input to the code accommodating any grid from a coarse 10 × 10 to a fine 190 × 190 grid. As the integration of Eq. (20) is a subset of that of Eq. (18)—one being only over a cone surrounding the peak and the other over the entire hemisphere—the numerical integration is performed over the cone first. For integration over the hemisphere, BRDF values of points within the cone are set to the minimum BRDF value at the intersection of the cone and the interpolated BRDF surface. The integration over the cone is then added to yield the approximation to Eq. (18).

The BRDF values at $\theta_r = 90$ deg are taken to be equal to the values at the largest measured θ_r for the same ϕ_r. The only exception to this rule is for 78 deg angle of incidence when application of the rule would entail extending the specular peak to $\theta_r = 90$ deg at $\phi_r = 180$ deg. In this case $\rho''(\theta_i = 78$ deg, $\phi_i = 0$ deg, $\theta_r = 90$ deg, $\phi_r = 180$ deg) is approximated by $\rho''(\theta_i = 78$ deg, $\phi_i = 0$ deg, $\theta_r = 78$ deg, $\phi_r = 170$ deg). BRDF data are also unavailable for incidence angles $\theta_i = 0$ and 90 deg due to instrument limitations at these angles. Rather than extrapolating from data near these angles, the approach taken here is to assume that values at 0 and 90 deg are identical to those at the nearest measured angle. The computer code was validated against exact results for a completely diffuse surface and one with a tractable single-lobed reflectance function. The agreement for the diffuse case is perfect for even the coarsest grid spacing. The lobed case shows agreement in directional-hemispherical reflectance to within 0.2% and agreement in the directional-specular reflectance to within 5%.

Specularity Results

Table 1 summarizes the specularity results for all twelve materials. The directional specularity, as defined in Eq. (11), is given as a function of angle of incidence and conical half angle at normal incidence $\beta_{c,o}$. The hemispherical specularity, as defined in Eq. (6), is also given as a function of $\beta_{c,o}$. Remember that $\beta_{c,o}$ is related to the particular conical half angle at θ_i by Eq. (17). The resulting hemispherical reflectance is also given in Table 1 and serves as a check for the results. In this study ρ and ρ' were not only needed to normalize the specularities but were also used to test the accuracy of the BRDF data and the resulting interpolated surface. Figure 4 shows the directional specularity results for five of the samples measured as a function of β_c. The results for black Kapton (Fig. 4a) indicate that, at 5 deg angle of incidence and β_c of 5 deg, the directional specularity is about 10%, increasing monotonically with angle of incidence to 92% at θ_i of 78 deg. Figure 4b shows that ITO-coated aluminized Kapton is strongly specular, with σ' greater than 72% for β_c of 5 deg and all angles of incidence. Comparison of Figs. 4c and 4d shows that the embossed silvered Teflon does have a reduced specularity, with values between 4–21% at β_c of 5 deg. Figure 4e shows results for white flat Chemglaze paint indicating very low specularity (<5%) up to β_c of 10 deg. These results are similar to those obtained for each of the flat paints at 0.488 μm. The results for white gloss Chemglaze paint are shown in Fig. 4f, where the σ' values rise rapidly to relatively low asymptotic values within the first 5 deg conical half angle. This effect is due to the substantial diffuse portion discussed earlier.

Figure 5a presents hemispherical specularity results for each of the six plastic films as a function of $\beta_{c,o}$. The least specular is the embossed silvered Teflon; the most specular is the ITO-coated aluminized Kapton, which spans a wide range from 2 to 70% at $\beta_{c,o}$ of 5 deg. Figure 5b shows σ as a function of $\beta_{c,o}$ for the painted samples measured at 0.488 μm. The black gloss paint is the most specular of these; comparison with Fig.

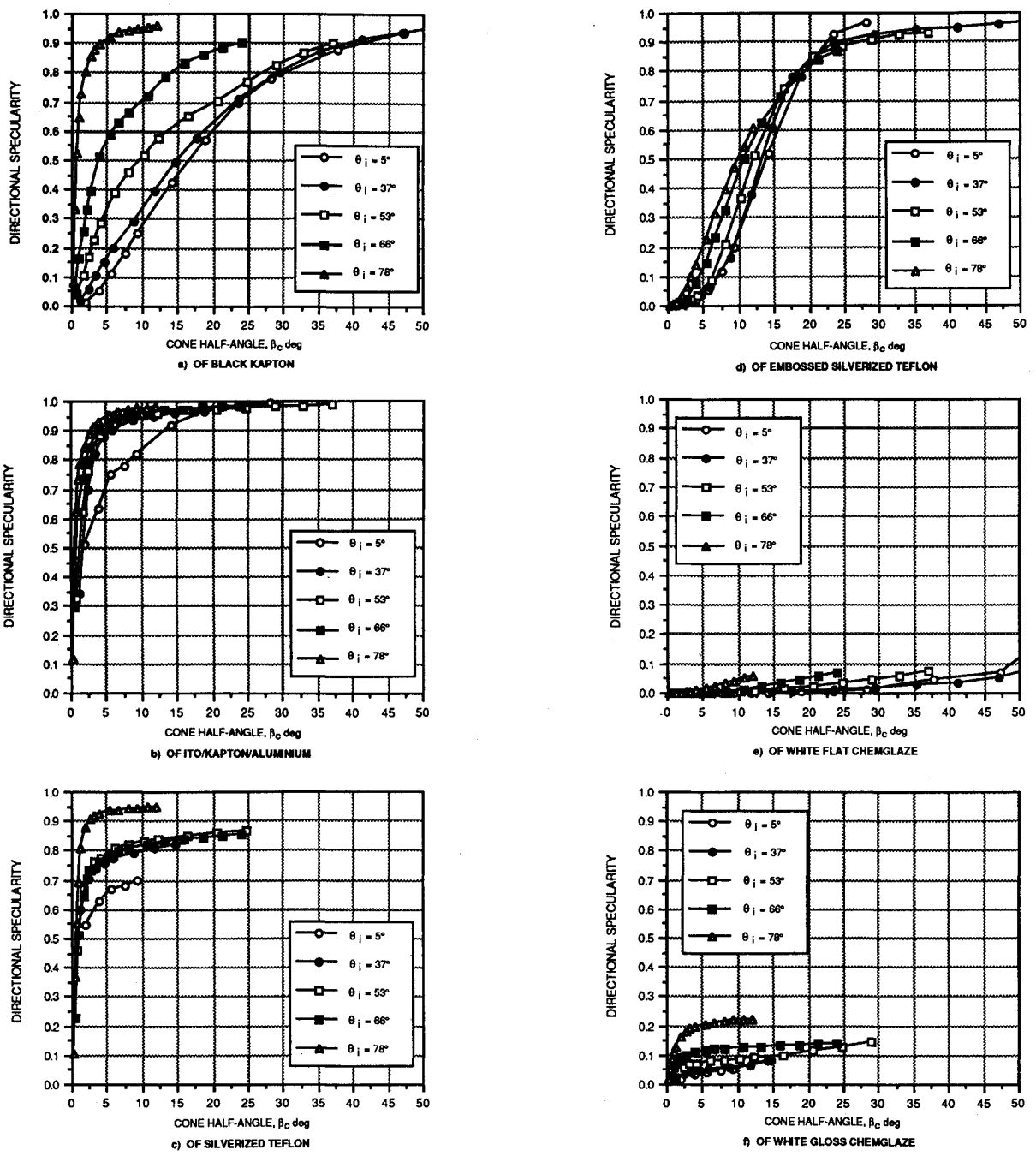

Fig. 4 Measured directional specularity.

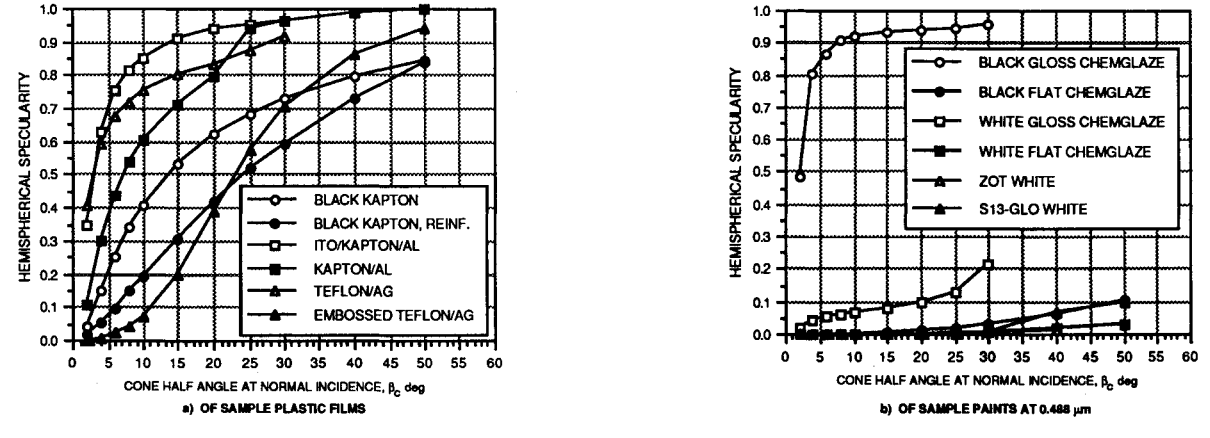

Fig. 5 Measured hemispherical specularity.

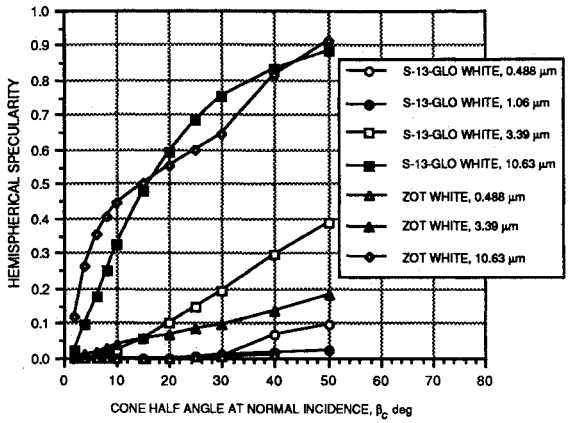

Fig. 6 Wavelength impact on hemispherical specularity of sample paints.

5a reveals that the black gloss paint was the most specular of all samples measured, including the metallized plastic films. The flat paints all have a σ of essentially zero until large conical half-angles (>25 deg) appear. Again, σ for the white gloss paint is relatively low (5–10%) because of the substantial diffuse portion. Figure 6 shows σ for the S13-GLO and ZOT white paints as a function of wavelength. At 0.488 and 1.06 μm the specularity is near zero. At 3.39 μm and $\beta_{c,o}$ of 10–20 deg, these paints are 5–10% specular, while at 10.63 μm, they are 30–60% specular.

Conclusions and Recommendations

Directional and hemispherical specularity of commonly used spacecraft thermal control materials can be accurately calculated by a method incorporating BRDF data. As expected, specularity tends to increase with both angle of incidence and wavelength. Each of the flat paints showed increased BRDF in the off-specular forward direction when measured at high angles of incidence. The most specular of the materials measured was a black gloss Chemglaze paint, a first-surface reflector. It is recommended that the study be extended to cover all of the external thermal control materials in use. BRDF measurements are needed at more wavelengths so that integrated solar specularities can be calculated. The BRDF and specularity data presented should be used to develop meaningful analytical models of surface reflectance for adaptation into spacecraft ray-trace Monte Carlo models.

Acknowledgments

This work was supported, in large part, by internal Hughes funding thanks to the efforts of L. A. Hennis. Thanks also go to J. May for the sample preparation, to W. Brennan and staff for the actual BRDF measurements, and to R. P. Bobco for his valuable counsel. Finally, thanks go to T. R. Moses for his diligence and patience in processing large quantities of data.

References

[1]Seban, R., "Discussion of 'An Enclosure Theory for Radiative Exchange Between Specularly and Diffusely Reflecting Surfaces' by Sparrow, E. M., Eckert, E. R. G., and Jonsson, V. K.," *Journal of Heat Transfer*, Vol. 84C, No. 4, 1962, pp. 299–300.

[2]Bobco, R. P., and Drolen, B. L., "Engineering Model of Surface Specularity: Spacecraft Design Implications," *Journal of Thermophysics and Heat Transfer*, Vol. 3, No. 3, 1989, pp. 289–296.

[3]Bennet, H. E., and Porteus, J. O., "Relation Between Surface Roughness and Specular Reflectance at Normal Incidence," *Journal of the Optical Society of America*, Vol. 51, No. 2, 1961, pp. 123–129.

[4]Birkebak, R. C., and Eckert, E. R. G., "Effects of Roughness of Metal Surfaces on Angular Distribution of Monochromatic Reflected Radiation," *Journal of Heat Transfer*, Vol. 87, Feb. 1965, pp. 85–94.

[5]Torrance, K. E., and Sparrow, E. M., "Biangular Reflectance of an Electric Non-Conductor as a Function of Wavelength and Surface Roughness," *Journal of Heat Transfer*, Vol. 87, No. 2, 1965, pp. 283–292.

[6]Torrance, K. E., Sparrow, E. M., and Birkebak, R. C., "Polarization, Directional Distribution, and Off-Specular Peak Phenomena in Light Reflected from Roughened Surfaces," *Journal of the Optical Society of America*, Vol. 56, No. 7, 1966, pp. 916–925.

[7]Smith, T. F., and Hering, R. G., *Surface Roughness Effects on Bidirectional Reflectance*, Univ. of Illinois Heat Transfer Lab., ME-TR-661-2, UILU-ENG-72-4001, Urbana-Champaign, IL, 1972.

[8]Funai, A. I., "Bidirectional Reflectance Measurements of Specular and Diffuse Surfaces With a Simple Spectrometer," *Heat Transfer and Thermal Control*, edited by A. L. Crosbie, Vol. 78, Progress in Astronautics and Aeronautics, AIAA, New York, 1981, pp. 25–48.

[9]Miller, W. D., "A Report on the Visual Bidirectional Reflectance Properties of Selected Apollo Materials," TRW Rept. 68-3346.11u-30 (NASA NAS9-5073), Redondo Beach, CA, April 1968.

[10]Siegel, R., and Howell, J. R., *Thermal Radiation Heat Transfer*, 2nd ed., Hemisphere, Washington, DC, 1981, pp. 64–72, 127–132, 142–145.

[11]Scheele, S. R., "Scattering from Infrared Transparent Materials," *Problems in Optical Systems, SPIE*, Vol. 107, *Stray Light*, April, 1977, pp. 48–56.

[12]IMSL MATH/LIBRARY, IMSL Inc., Version 1.0, MALB-USM-UNBND-1.0, Vol. 2, Houston, TX, April 1987, Chap. 3, pp. 516–519.